nature climate change

LETTERS

https://doi.org/10.1038/s41558-018-0236-4

Projected increases and shifts in rain-on-snow flood risk over western North America

Keith N. Musselman[1*], Flavio Lehner[2], Kyoko Ikeda[2], Martyn P. Clark[2], Andreas F. Prein[2], Changhai Liu[2], Mike Barlage[2] and Roy Rasmussen[2]

Destructive and costly flooding can occur when warm storm systems deposit substantial rain on extensive snowcover[1–6], as observed in February 2017 with the Oroville Dam crisis in California[7]. However, decision-makers lack guidance on how such rain-on-snow (ROS) flood risk may respond to climate change. Here, daily ROS events with flood-generating potential[8] are simulated over western North America for a historical (2000–2013) and future (forced under Representative Concentration Pathway 8.5[9]) period with the Weather Research and Forecasting model; 4 km resolution allows the basin-scale ROS flood risk to be assessed. In the warmer climate, we show that ROS becomes less frequent at lower elevations due to snowpack declines, particularly in warmer areas (for example, the Pacific maritime region). By contrast, at higher elevations where seasonal snowcover persists, ROS becomes more frequent due to a shift from snowfall to rain. Accordingly, the water available for runoff[10] increases for 55% of western North American river basins, with corresponding increases in flood risk of 20–200%, the greatest changes of which are projected for the Sierra Nevada, the Colorado River headwaters and the Canadian Rocky Mountains. Thus, flood control and water resource planning must consider ROS to fully quantify changes in flood risk with anthropogenic warming.

In the western United States and Canada, 85 million people are reliant on rivers and reservoirs to transport and store mountain snow water resources[11,12]. Many of these water systems are prone to large rain-on-snow (ROS) flood events[3]. Compared to the equivalent heavy rainfall on a snow-free landscape, ROS can enhance the flood risk due to additional runoff from snowmelt. The combined heavy rainfall and snowmelt can cause a rapid hydrologic response[13,14] that can generate floods of substantial consequence. Recent examples include the February 2017 near-failure of the Oroville Dam in California that led to evacuations of about 190,000 people[7], and a June 2013 flood in Alberta, Canada, that was the costliest natural disaster in Canadian history[6].

Despite the socioeconomic impact of ROS floods, little is known about how ROS events vary in time, spatial extent and intensity across large mountainous areas. Even less is known about how ROS flood risk may respond to warming. Mid-century projections of changes in ROS frequency over North America with regional climate models[15] predict increases at northern latitudes (>50° N) due to more frequent winter rainfall and declines at lower latitudes due to less snowcover. Historical observations (1949–2003) of ROS frequency in the western United States[3] confirm that an analogous trend has occurred over elevation gradients with declines at lower elevations and increases at higher elevations. Together with similar trends in Europe[8], the historical evidence indicates that ROS characteristics are undergoing large-scale transformations in response to warming-induced changes in snowcover and precipitation phase[16]. The strong climate- and elevation-dependent sensitivity of ROS suggests that model simulations must be conducted at sufficiently high resolution to represent climatic and orographic gradients of precipitation magnitude and phase, and snowpack formation, persistence and melt in mountainous regions.

There is scientific consensus that flood regimes in historically snow-dominated mountainous regions will shift from spring snowmelt-driven events toward more frequent rain-dominated winter floods[17,18]. However, such estimates are based on coarse resolution (>50 km) models with limited ability to resolve orographic gradients of rainfall intensity[19] and snowpack development[20]. Importantly, ROS flood risk is largely determined by antecedent snowpack conditions, which vary greatly with elevation[2,21–23]. Where the snowpack is deep, such as at high elevations, rainfall can be buffered while the snowpack warms to melting temperature and reaches relative saturation, thus reducing runoff[2]. Conversely, a shallow snowpack will minimally contribute to total runoff. Thus, prime conditions for a ROS flood include heavy rain occurring on an extensive snowpack and resulting in sufficient melt to contribute to runoff.

We present an analysis of daily ROS events with flood potential simulated at high resolution (4 km horizontal grid spacing; Supplementary Fig. 1) over western North America using the Weather Research and Forecasting (WRF) model. Two 13-year simulations were used: a historical reanalysis (2000–2013), verified against an observationally constrained snow model (Supplementary Fig. 2), and a pseudo-global warming climate simulation (see Methods and ref. [24]). In the latter, the weather of the current climate is assumed to reoccur under a concentration pathway where end-of-century radiative forcing increases by +8.5 W m^{-2}. We define daily ROS with flood-generating potential (hereafter, ROS) as heavy rainfall ≥10 mm d^{-1} falling on snowpack ≥10 mm snow water equivalent (SWE), where the sum of rainfall and snowmelt contains ≥20% snowmelt[8]. The definition lends confidence that daily ROS events satisfying these thresholds have the potential to cause consequential flooding (see Methods).

In our analysis, we focus on three primary mechanisms that can affect ROS flood potential in a warmer climate: (1) reduced snowcover persistence[25] decreasing ROS frequency and spatial extent, (2) a greater proportion of annual precipitation falling as rain on a pre-existing snowpack[26] increasing ROS frequency and spatial extent, and (3) more intense rainfall[27] and/or snowmelt increasing ROS intensity. We assess how these change mechanisms interact and combine over elevation gradients to impact future ROS water

[1]Institute of Arctic and Alpine Research, University of Colorado Boulder, Boulder, CO, USA. [2]The National Center for Atmospheric Research (NCAR), Boulder, CO, USA. *e-mail: keith.musselman@colorado.edu

available for runoff. Finally, we assess projected changes in basin-scale potential runoff from the ten largest ROS events simulated in the historical and warmer climate scenarios. We present the first high-resolution process representation necessary to understand how this major flood hazard may respond to climate change over large mountainous areas.

In the historical period, the frequency of ROS events varies greatly over western North America (Fig. 1a) consistent with historical observations[3]. The spatial distribution is determined by the regional climatology of precipitation, temperature and snowcover persistence, all of which are largely governed by elevation[28]. Historical ROS is most frequent (darker colours in Fig. 1a) along mountain ranges inland of the Pacific Ocean coasts. In this maritime climate, winter storms can bring alternating deep accumulating snowfall and heavy rain, depending on the elevation, freezing level heights and storm track. These conditions, together with the high frequency of winter rainfall (Supplementary Fig. 2a), are most likely to form the antecedent snowpack and rainfall conditions that can generate ROS flooding. Conversely, ROS is least frequent (white to grey colours in Fig. 1a) at lower elevations, in drier regions where seasonal snowpack is rare, and in higher-elevation and/or more continental mountain ranges.

In the warmer scenario, ROS events are less frequent at lower elevations and more frequent at middle elevations, particularly in the warmer maritime regions (Figs. 1b,c and 2). Figure 2 shows that reductions in ROS frequency are explained by substantial snowpack losses. This is inferred from the large reductions at lower elevations in the number of days with SWE $\geq$ 10 mm (Fig. 2). Conversely, increases in ROS frequency at middle elevations are explained by a warming-induced precipitation phase shift from snowfall in the historical climate to rain in the warmer scenario. This is inferred from large increases at middle elevations in the fraction of heavy precipitation days occurring as rainfall (Fig. 2). The ROS frequency changes are progressively dampened with distance from the coast. Little ROS frequency change occurs at elevations of >2,500 m a.s.l. (Supplementary Fig. 1), despite large reductions in snowcover duration. This suggests that the colder climate of the higher elevations inhibits the ROS frequency reductions projected for warmer regions[29].

Historical average daily ROS intensity (that is, the water available for runoff from rainfall and snowmelt) is highest in the Pacific maritime mountains and parts of the northern Rockies and is lowest in colder continental climates such as the Rocky Mountains, Prairies and Plains (Fig. 3a). Warming increases ROS intensity (Fig. 3b) and the change (Fig. 3c) is largely explained by increases in rainfall during ROS events (Fig. 3d) rather than increases in snowmelt intensity (Fig. 3e). Changes in the snowmelt contribution to total ROS runoff are highly variable, with slight increases in maritime regions and moderate reductions in the northern Rockies (Fig. 3e). The historical contribution of snowmelt to total ROS runoff (that is, rainfall plus snowmelt) varies greatly over western North America (Fig. 3f), with the largest contributions (45% to >65%) in the Rocky Mountains and the lowest contributions (30% to 45%) in the maritime regions. These regional differences are probably explained by differences in ROS seasonality and precipitation climatology (see Methods and Supplementary Fig. 3). How changes in rainfall and snowmelt intensity may impact the ROS flood hazard in individual river basins demands a joint consideration of changes in ROS frequency, intensity and the antecedent snowpack conditions.

Large increases in the top 10 daily ROS events are projected for many mountainous regions of western North America (Fig. 4a). The top 10 events are calculated as the ranked daily ROS runoff volumes aggregated to river basins and computed separately for each basin and simulation (see Methods). In 58 of the 106 major river basins (55%) that received at least 10 ROS events in both simulation periods, average event runoff increased by >20%. In 20 of the basins, or ~17% of western North America, ROS runoff increased by >100% (Fig. 4a). In the warmer climate, basin event runoff volumes increase by 20% to >100% for the Cascade Mountains, the northern Sierra Nevada, interior British Columbia and the Canadian Rockies, and by >200% for central and southern Sierra Nevada basins and the Colorado River headwaters (Fig. 4a).

The increases in ROS event runoff are strongly and positively related to changes in the spatial extent of the top 10 ROS events (Fig. 4b), with only minor contribution from changes in ROS intensity (Fig. 4c; see scatter plot of Fig. 4d). Changes in runoff volume are also positively related to changes in the average elevation range of the top 10 ROS events (see Methods and Fig. 4e). Thus, increases in total ROS runoff volume are associated with increases in the spatial extent of ROS events, which are explained by an upward expansion of ROS to include higher elevations.

Conversely, little change to large declines in the average runoff from the top 10 ROS events are projected for lower elevation basins, such as along the Pacific coast, the US Southwest and some inland basins (Fig. 4a). These changes are explained by ROS frequency reductions due to snowcover depletion (Figs. 1 and 2) consistent with historical observations[3] and continental-scale projections[15]. However, the results shown in Fig. 4 do not include rainfall on snow-free ground. Rainfall intensity is projected to increase in a warmer climate (Fig. 3f) and will affect a greater basin area due

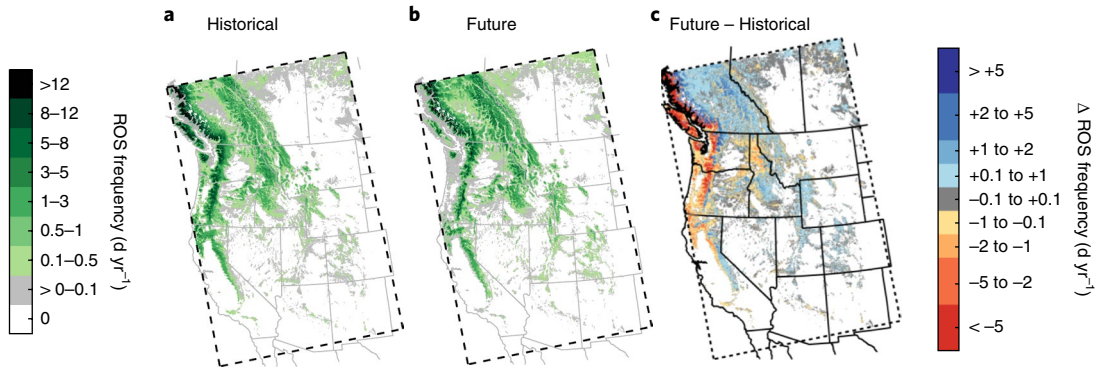

Fig. 1 | In a warmer climate, ROS will be less frequent at lower elevations, particularly in warmer regions, and more frequent at middle elevations and in historically colder regions. a,**b**, Average annual frequency of ROS meeting the 'flood potential' thresholds in the historical control period (2000–2013) (**a**) and future warming scenario (**b**). **c**, Difference in ROS frequency. Colour bars are nonlinear for improved visual interpretation. Dashed lines indicate the analysis region.

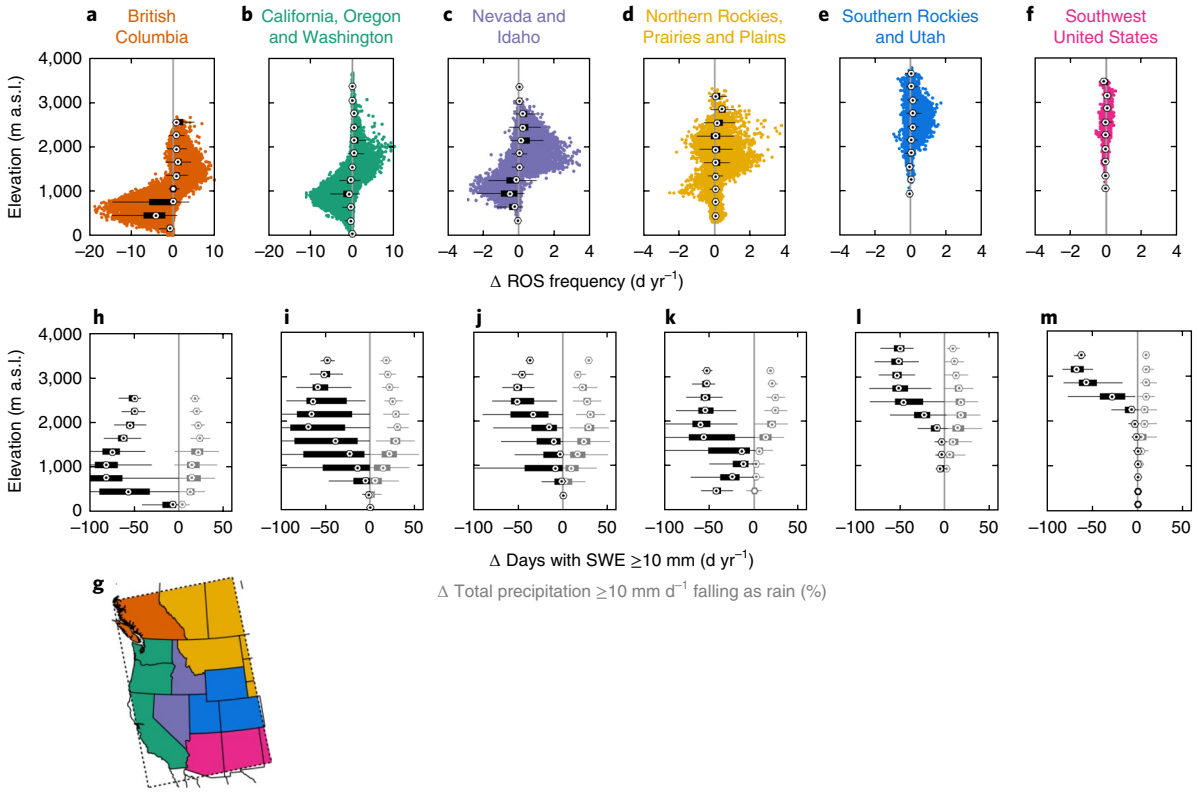

Fig. 2 | Warming reduces ROS frequency at lower elevations due to snowpack loss and increases ROS frequency at higher elevations due to a shift from snowfall to rain. a–m, Elevation distribution of the changes in ROS frequency (Fig. 1c) (**a–f**) for geographical regions (**g**) and change in days with SWE ≥ 10 mm (black boxplots) (**h–m**) and the fraction of precipitation ≥10 mm d^{-1} as rain (grey boxplots). Boxplots show medians (circles), interquartile ranges (box widths) and extreme data points (whiskers) in 300 m elevation bands. Note the differences in the *x* axis scales between coastal (**a**,**b**) and inland regions (**c–f**).

to a precipitation phase shift from snowfall to rain[30]. Thus, basins with negligible or negative changes in top 10 ROS event volumes (Fig. 4a) could be interpreted as basins where the flood potential shifts from ROS-driven to rainfall-driven. Furthermore, in the warmer scenario, the top 10 ROS events are projected to occur up to three months earlier than those of the historical period. Thus, climate change will shift the ROS flood potential from spring to winter (Fig. 4f and Supplementary Fig. 3), consistent with global projections of river flood risk[17,18].

We assess historical and projected future water available for runoff produced by daily ROS of sufficient magnitude to generate a potential flood. We do not simulate actual flood events. More work is needed to understand how soil ice and moisture content combine with event timing and catchment-integrated water to impact streamflow and downstream flooding. Future hydrologic simulations that better promote analysis of hydrologic events and direct impact studies that include representation of water management infrastructure are needed to translate our results into actionable information for decision-makers and stakeholders.

We present an analysis of ROS events with flood-generating potential over western North America simulated by the WRF model for a 13-year control period and a future climate scenario. The high resolution of the WRF simulations permitted an assessment of how the antecedent snowpack conditions and rainfall intensity required to generate a ROS flood may change with anthropogenic warming. We have two primary findings. First, in a warmer climate, ROS is less frequent at lower elevations, particularly in warmer regions, and is more frequent at higher elevations. Reductions in ROS frequency at lower elevations are due to antecedent snowpack losses, and increases at higher elevations where snowcover persists are caused by a shift from snowfall to rain. Second, the water available for runoff from the 10 largest ROS events simulated in 106 major river basins substantially declines for more than one-quarter of the basins, increases by > 20% for more than half of the basins, and more than doubles for nearly 20% of western North American river basins. These projected spatial shifts in rain-on-snow flood risk have not been previously reported. The increases are caused by a spatial expansion of ROS events to include larger elevation ranges and slight increases in ROS intensity.

Our results suggest that increases in ROS water available for runoff coupled with a greater proportion of precipitation falling as rain, and increased rainfall intensity, should be considered in flood control planning. The largest increases in ROS runoff are projected for mountainous river basins that are historically prone to flooding and/or in regions where the storage and transport of snow water resources are paramount. For example, the water volume produced by the most intense daily ROS events simulated for the Sacramento River basin in California is projected to increase by >20% in the warmer climate scenario. This basin contains the Oroville Dam, which was critically damaged by emergency water releases during a 2017 ROS event. This river basin and many others we highlight include some of the largest metropolitan regions in western North America, underscoring the potential societal and economic impacts of the projected changes. Thus, flood control and reservoir management systems in these mountainous regions must consider future changes in rain-on-snow events to fully quantify changes in basin-scale flood risk with anthropogenic warming.

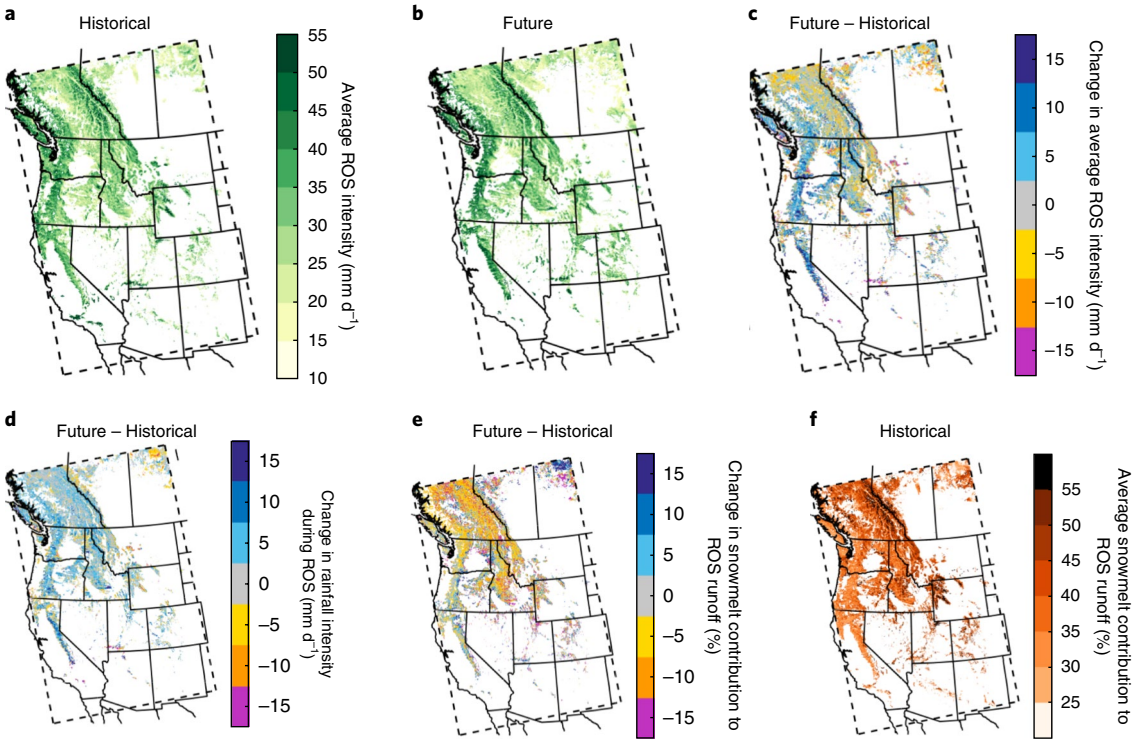

Fig. 3 | For many mountainous regions, future rain-on-snow events will be more intense, largely due to increases in rainfall rather than snowmelt increases. a–c, Average daily intensity of ROS runoff (rainfall + snowmelt) meeting the flood potential thresholds in the historical period (**a**) and future scenario (**b**) and the difference in ROS intensity between the two scenarios (**c**). **d**,**e**, Projected changes in average rainfall intensity during ROS events (**d**) and snowmelt contribution to total ROS runoff (rainfall + snowmelt) (**e**). **f**, Historical average snowmelt contribution to ROS runoff.

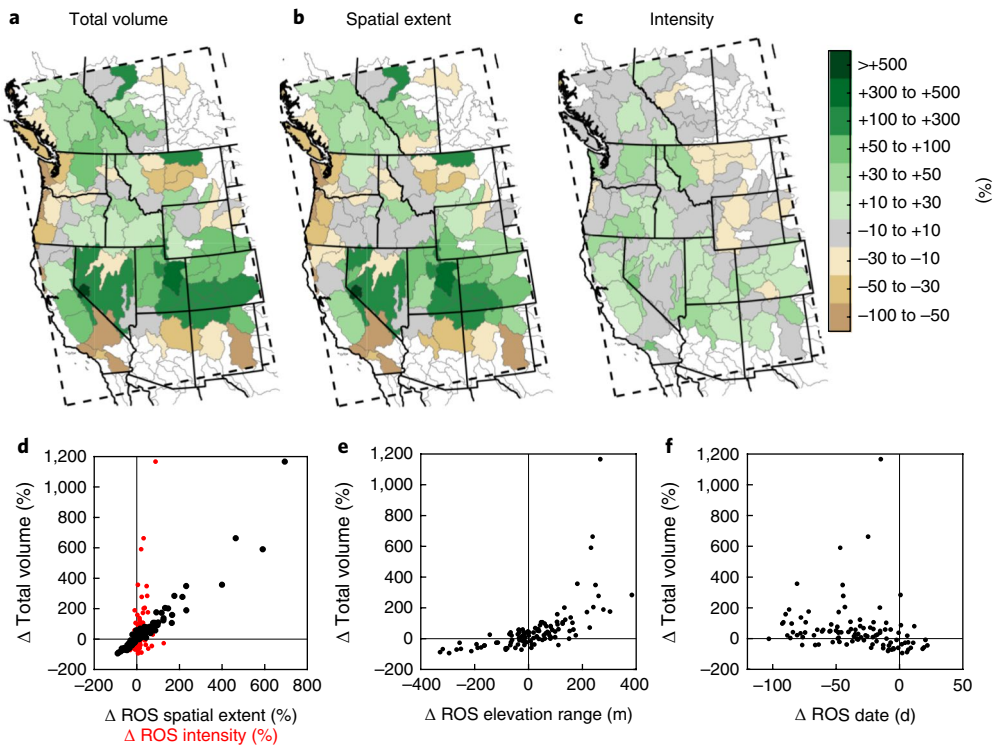

Fig. 4 | Increases in the ROS flood potential are projected, explained by a spatial expansion of ROS to include higher elevations and slight increases in rainfall intensity. a–c, Changes in simulated ROS total volume (**a**), spatial extent (**b**) and intensity (**c**) for the top 10 ROS events for major river basins. **d–f**, Scatter plots of the change in total volume for all basins versus the changes in spatial extent (black) and intensity (red) (**d**), change in elevation range (**e**) and change in ROS date (**f**). Data points for Δ ROS total volume, spatial extent and intensity in **d–f** correspond to the basins mapped in **a–c**.

Methods

Methods, including statements of data availability and any associated accession codes and references, are available at https://doi.org/10.1038/s41558-018-0236-4.

Received: 21 November 2017; Accepted: 2 July 2018;
Published online: 06 August 2018

References

1. Kattelmann, R. Flooding from rain-on-snow events in the Sierra Nevada. *IAHS Publ. Ser. Proc. Rep. Intern Assoc. Hydrol. Sci.* **239**, 59–66 (1997).
2. Marks, D., Kimball, J., Tingey, D. & Link, T. The sensitivity of snowmelt processes to climate conditions and forest cover during rain-on-snow: a case study of the 1996 Pacific Northwest flood. *Hydrol. Process.* **12**, 1569–1587 (1998).
3. McCabe, G. J., Hay, L. E. & Clark, M. P. Rain-on-snow events in the western United States. *Bull. Am. Meteorol. Soc.* **88**, 319–328 (2007).
4. Berghuijs, W. R., Woods, R. A., Hutton, C. J. & Sivapalan, M. Dominant flood generating mechanisms across the United States. *Geophys. Res. Lett.* **43**, 4382–4390 (2016).
5. Merz, R. & Blöschl, G. A process typology of regional floods. *Water Resour. Res.* **39**, 1340 (2003).
6. Pomeroy, J. W., Stewart, R. E. & Whitfield, P. H. The 2013 flood event in the South Saskatchewan and Elk River basins: causes, assessment and damages. *Can. Water Resour. J.* **41**, 105–117 (2016).
7. Vahedifard, F., AghaKouchak, A., Ragno, E., Shahrokhabadi, S. & Mallakpour, I. Lessons from the Oroville dam. *Science* **355**, 1139–1140 (2017).
8. Freudiger, D., Kohn, I., Stahl, K. & Weiler, M. Large-scale analysis of changing frequencies of rain-on-snow events with flood-generation potential. *Hydrol. Earth Syst. Sci.* **18**, 2695 (2014).
9. Riahi, K. et al. RCP 8.5—a scenario of comparatively high greenhouse gas emissions. *Climatic Change* **109**, 33–57 (2011).
10. Mazurkiewicz, A. B., Callery, D. G. & McDonnell, J. J. Assessing the controls of the snow energy balance and water available for runoff in a rain-on-snow environment. *J. Hydrol.* **354**, 1–14 (2008).
11. Li, D., Wrzesien, M. L., Durand, M., Adam, J. & Letternmaier, D. P. How much runoff originates as snow in the western United States, and how will that change in the future?. *Geophys. Res. Lett.* **44**, 6163–6172 (2017).
12. Sturm, M., Goldstein, M. A. & Parr, C. Water and life from snow: a trillion dollar science question. *Water Resour. Res.* **53**, 3534–3544 (2017).
13. Eiriksson, D. et al. An evaluation of the hydrologic relevance of lateral flow in snow at hillslope and catchment scales. *Hydrol. Process.* **27**, 640–654 (2013).
14. Singh, P., Spitzbart, G., Hübl, H. & Weinmeister, H. Hydrological response of snowpack under rain-on-snow events: a field study. *J. Hydrol.* **202**, 1–20 (1997).
15. Jeong, D. I. & Sushama, L. Rain-on-snow events over North America based on two Canadian regional climate models. *Clim. Dynam.* **50**, 303–316 (2018).
16. Barnett, T. P., Adam, J. C. & Lettenmaier, D. P. Potential impacts of a warming climate on water availability in snow-dominated regions. *Nature* **438**, 303–309 (2005).
17. Arnell, N. W. & Gosling, S. N. The impacts of climate change on river flood risk at the global scale. *Climatic Change* **134**, 387–401 (2016).
18. Hirabayashi, Y. et al. Global flood risk underclimate change. *Nat. Clim. Change* **3**, 816–821 (2013).
19. Prein, A. F. et al. Importance of regional climate model grid spacing for the simulation of heavy precipitation in the Colorado headwaters. *J. Clim.* **26**, 4848–4857 (2013).
20. Ikeda, K. et al. Simulation of seasonal snowfall over Colorado. *Atmos. Res.* **97**, 462–477 (2010).
21. Wayand, N. E., Lundquist, J. D. & Clark, M. P. Modeling the influence of hypsometry, vegetation, and storm energy on snowmelt contributions to basins during rain-on-snow floods. *Water Resour. Res.* **51**, 8551–8569 (2015).
22. Jennings, K. & Jones, J. A. Precipitation-snowmelt timing and snowmelt augmentation of large peak flow events, western Cascades, Oregon. *Water Resour. Res.* **51**, 7649–7661 (2015).
23. Musselman, K. N., Molotch, N. P., & Margulis, S. A.. Snowmelt response to simulated warming across a large elevation gradient, southern Sierra Nevada, California. *Cryosphere* **11**, 2847–2866 (2017).
24. Liu, C. et al. Continental-scale convection-permitting modeling of the current and future climate of North America. *Clim. Dynam.* **49**, 71–95 (2017).
25. Mote, P. W., Hamlet, A. F., Clark, M. P. & Lettenmaier, D. Declining mountain snowpack in western North America. *Bull. Am. Meteorol. Soc.* **86**, 39–49 (2005).
26. Knowles, N., Dettinger, M. D. & Cayan, D. R. Trends in snowfall versus rainfall in the Western United States. *J. Clim.* **19**, 4545–4559 (2006).
27. Trenberth, K. E. Changes in precipitation with climate change. *Clim. Res.* **47**, 123–138 (2011).
28. Trujillo, E. & Molotch, N. P. Snowpack regimes of the Western United States. *Water Resour. Res.* **50**, 5611–5623 (2014).
29. Rasmussen, R. et al. High-resolution coupled climate runoff simulations of seasonal snowfall over Colorado: a process study of current and warmer climate. *J. Clim.* **24**, 3015–3048 (2011).
30. Hamlet, A. F. & Lettenmaier, D. P. Effects of 20th century warming and climate variability on flood risk in the western US. *Water Resour. Res.* **43**, W06427 (2007).

Acknowledgements

The National Center for Atmospheric Research (NCAR) is sponsored by the National Science Foundation (NSF). K.N.M. was supported under an NCAR Advanced Study Program (ASP) Postdoctoral Fellowship. F.L. was supported by a Postdoc Applying Climate Expertise (PACE) fellowship co-sponsored by the National Oceanic and Atmospheric Administration and the Bureau of Reclamation, administered by Cooperative Programs for the Advancement of Earth System Science (CPAESS). The authors acknowledge high-performance computing support from Yellowstone (ark:/85065/d7wd3xhc) provided by NCAR's Computational and Information Systems Laboratory, sponsored by the NSF. The authors also thank N. Mizukami, A. Newman and E. Gutmann for discussions.

Author contributions

All authors designed the study. K.N.M. conducted the analysis. C.L. ran the WRF simulations. K.I. managed the WRF output. M.B. customized the WRF output that facilitated ROS analysis. K.N.M., F.L., A.F.P. and M.P.C. contributed to the interpretations of the results. K.N.M., F.L., A.F.P., M.P.C. and R.R. wrote the paper.

Competing interests

The authors declare no competing interests.

Additional information

Supplementary information is available for this paper at https://doi.org/10.1038/s41558-018-0236-4.

Reprints and permissions information is available at www.nature.com/reprints.

Correspondence and requests for materials should be addressed to K.N.M.

Publisher's note: Springer Nature remains neutral with regard to jurisdictional claims in published maps and institutional affiliations.

Methods

WRF simulations. *Model set-up.* We analyse results from a high-resolution (4 km), 13-year (October 2000 to September 2013) retrospective simulation with WRF model Version 3.4.1 run over much of North America. Initial and boundary conditions were specified from ERA-Interim reanalysis data[31]. The improved Noah-MP land surface model[32] simulated the surface energy and water balance, including snowpack dynamics and vegetation–snow interactions. Critically, a microphysics-based rain–snow partitioning scheme in WRF replaced the more common and subjective temperature-based approach known to introduce uncertainty in snow models[33]. The Noah-MP physics developments significantly improve the WRF model skill by increasing the seasonal snowpack amount and decreasing cold biases over snow-covered areas[24]. For the detailed model configuration the reader is referred to ref. [24].

Hourly model output was cropped from the native domain of 1,360 × 1,016 grid points to a subdomain of 435 × 664 grid points (1,740 km east–west by 2,656 km north–south) covering the western United States and southwestern Canada and aggregated to daily values (midnight Pacific Standard Time or UTC-8)[34]. The land surface model had an upper SWE limit of 2,000 mm, which was typically exceeded over glaciated regions. Because the model did not include glacier dynamics, pixels that exceeded this threshold in any year of either scenario were excluded from the analysis[34].

Verification. Realistic simulation of ROS requires accurate estimates of precipitation magnitude and phase (that is, whether precipitation is liquid or frozen), the snowpack magnitude, the snowpack energy balance required to simulate snowmelt rates, and an accurate representation of the co-occurrence of SWE and rainfall. Previous evaluations of the historical WRF reanalysis data show good skill in representing many of these processes: good agreement with measurements have been shown for mountain precipitation magnitude[24], storm track[35], heavy rainfall[36] and snowmelt rates[34]. For detailed validation of simulated precipitation at mountain snowpack telemetry sites, see ref. [24]. For verification of simulated snowmelt rates, see ref. [34]. The simulated patterns of ROS event frequency and seasonality are similar to station observations reported over the western United States[3]. The good correspondence between historical measured and modelled precipitation, snowpack, snowmelt and general ROS patterns provides confidence in the model representation of daily ROS events.

As an additional verification, we provide an assessment of the spatial distribution and frequency of the ROS variables that comprise the thresholds we use to define ROS events with flood potential (see section 'Daily ROS event definition'). We compare the metrics simulated by WRF to those simulated by a snow data assimilation model system (SNODAS)[37] operated by the National Operational Hydrologic Remote Sensing Center (NOHRSC), part of the National Weather Service and the National Oceanic and Atmospheric Administration (NOAA). The comparison is made for a period when both data sets were available (1 October 2003 to 30 September 2013) and for a common geographic region of western North America.

Supplementary Fig. 2 includes maps of the average annual frequency of rainfall ≥10 mm, SWE ≥10 mm, the co-occurrence of both thresholds being satisfied, and, finally, three thresholds: the previous two and melt ≥20% of the total potential runoff. Both models show similar general patterns and magnitudes of the frequency of rainfall, SWE and ROS events. There are also discrepancies between the models. While SNODAS is run on a 1 km grid, the forcing data have a native resolution[37] up to an order of magnitude coarser than the 4 km WRF simulations. Thus, WRF is likely to resolve more detailed precipitation and snowpack processes in mountain regions, as can be inferred from Supplementary Fig. 2—note the finer scale variability of rainfall and SWE in WRF (Supplementary Fig. 2a,d,g,j) compared to SNODAS (Supplementary Fig. 2b,e,h,k)—and highlighted in the difference maps (Supplementary Fig. 2c,f,i,l). Compared to WRF, SNODAS simulates a higher frequency of ROS in most mountainous regions (Supplementary Fig. 2i,l), possibly due to prolonged snowcover duration relative to WRF (Supplementary Fig. 2f). While the reasons for the model discrepancies are not clear, and are beyond the scope of this study, the comparison suggests that WRF may be more conservative in its ROS estimation than SNODAS.

We conclude that WRF is capable of simulating ROS, especially in mountainous regions, and emphasize that this is the first high-resolution climate change analysis of ROS events. Improved observational data sets of ROS processes including in-snow meltwater storage and transport, and additional modelling studies that include processes such as wind effects on snow redistribution[38] known to determine regional snowcover persistence[39], should improve predictive capacity and constrain uncertainty related to ROS flood risk in present and future climates.

We also conducted an analysis to test whether the historical winter (NDJFMA) period from November 2000 to April 2013 simulated in our study is representative of the longer-term (January 1981 to December 2015) climate. We analysed the observationally derived daily precipitation and temperature data from the Parameter-elevation Relationships on Independent Slopes Model (PRISM; ref. [40]; available online from http://prism.oregonstate.edu/recent/). PRISM is available at 30 arcsec (~800 m) grid spacing for the conterminous United States. It is representative of the current state of knowledge of spatial climate patterns in the United States[40].

We investigated the top 100 precipitation events in each subregion (limited to the US portion of the domain) that occurred in the winter (November, December, January, February, March, April) when rain-on-snow is most common (see seasonality in Supplementary Fig. 3 and discussed below). Daily precipitation values were computed as the subregion average daily rate for all subregion grid cells. For each event, we also computed the mean air temperature within the subregion. Supplementary Fig. 4 shows that there are no statistically significant long-term trends in the top 100 daily precipitation events within the five subregions. The mean and variance of the precipitation extremes in the simulation period are not statistically distinguishable from the climatology (see histogram in Supplementary Fig. 5). Furthermore, there is neither a significant trend in the air temperatures at which the top 100 precipitation events occur (Supplementary Fig. 6) nor is the 2 m air temperature during the top 100 precipitation days within the simulation period statistically distinguishable from climatology (Supplementary Fig. 7). In summary, our 2000–2013 simulation period is representative of the 1981–2015 climatology.

Future projection. A climate perturbation experiment was conducted to simulate future (2071–2100) climate sensitivity to the Representative Concentration Pathway (RCP) 8.5 emission scenario[9], in which greenhouse gas emissions continue to increase through the twenty-first century. Like the pseudo-global-warming (PGW) method[41] used in previous WRF runs over Colorado[29,42], six-hourly ERA-Interim reanalysis conditions from the control experiment were perturbed by a climate change delta by adding monthly mean temperature, moisture and circulation change between the periods 1976–2005 and 2071–2100 from an ensemble of 19 CMIP5 models. Details of the model configuration are provided in ref. [24].

The applied PGW method assumes that much of the storm track, timing and successive weather type progression simulated in the historical climate is maintained in the warmer climate. Thus, potential changes in storm track position or frequency that could change historical precipitation patterns and variability are not fully addressed. Indeed, future projections of such dynamic changes remain highly uncertain[43], although a widespread increase in precipitation variability on all timescales is expected, driven by a combination of dynamic and thermodynamic changes[44]. The close correspondence of the PGW framework with historically observed weather[24] represents a pragmatic investigation of the isolated and better-understood influences of warming on thermodynamic processes as they impact precipitation, snowpack and snowmelt as all climate models predict increases in temperature and moisture. Our results are based on this robust future climate change signal for one plausible greenhouse gas emissions scenario.

Daily ROS event definition. Daily ROS with flood-generating potential is defined as heavy rainfall of at least 10 mm d^{-1} falling on snowpack of at least 10 mm snow water equivalent (SWE), where the sum of rainfall and snowmelt contains at least 20% snowmelt[8]. Following descriptive indices for extreme precipitation[45], the 10 mm d^{-1} rainfall intensity threshold, classified as heavy rainfall, is more conservative than the 3 mm over 6 days threshold value used in a previous large-scale analysis of ROS in Europe[8], and a 6.1 mm d^{-1} threshold used in a US Pacific Northwest study designed to include 'small ROS events'[10]. Our more conservative definition lends confidence that an identified (daily) ROS event has the potential to cause consequential flooding. Furthermore, the 20% snowmelt threshold ensures that cold content is eliminated and snow water storage capacity is exceeded, guaranteeing substantial drainage from the snowpack base[46] and that snowmelt contributes substantially to potential flood generation[8]. For example, snowmelt during ROS conditions in the Pacific maritime regions of the United States and Canada can add 25%[10,47] to >50%[2] to the rainfall input. Our 20% threshold is lower than these published values.

The median and standard deviation of the snowmelt contribution as a percent of total runoff simulated in the historical case with and without the 20% threshold was 43 ± 9% (mapped in Fig. 3f) and 38 ± 16% (not shown). The close correspondence of the two median values suggests that most ROS events that met the 10 mm rainfall threshold also met the 20% threshold. Tests with lower threshold values (rainfall and snowmelt contribution) did not change the general patterns or conclusions that we report. Tests with higher threshold values reduced the sample size and robustness of results, particularly in regions where ROS is less intense. The snowmelt contribution values mapped in Fig. 3f are consistent with those reported in ROS case studies. For example, values of 30 to 45% are commonly reported in California and the US Pacific Northwest[2,10], and values of >65% have been reported[2], which are consistent with the upper limit of our simulated values (Fig. 3f).

While ROS flood events can persist for multiple days to nearly a week[2,6,8,47], we evaluate daily ROS water available for runoff rather than multi-day event totals. In a model reanalysis of historical ROS events in Europe, the authors of ref. [8] used rainfall (>3 mm d^{-1}) and snowmelt (>20% total runoff volume) thresholds to mark the start of an event, and subsequent declines in observed streamflow to index the end of that event, which could be many days later. By using a daily ROS definition, rather than a multi-day event definition, we avoid ambiguities that could result from changes in event classification between the historical and warmer scenarios. For example, a long-duration event in the historical scenario may split into

multiple events in the warmer scenario, or vice versa. Our daily definition ensures consistency between scenarios that the simulated flood generating potential is driven predominantly by rain-on-snow.

Seasonal analysis of historical and future ROS events. The seasonality of ROS events was evaluated for the historical and warmer scenarios (Supplementary Fig. 3). For each scenario, the daily ROS frequency was categorized into autumn, winter and spring seasons, corresponding to months ASON, DJFM and AMJJ, respectively. The average annual dominant seasonality was computed as the percentage of relative frequency for each season divided by the total ROS frequency (shading and colours in Supplementary Fig. 3). In the historical period, springtime ROS was dominant (80–100%) in continental regions such as the Rocky Mountains. Conversely, winter ROS was dominant at lower elevations in interior British Columbia and middle to upper elevations in the Pacific Maritime regions including the Sierra Nevada (Supplementary Fig. 3). In the warmer climate, ROS that historically occurred in spring tended to shift towards winter, particularly in the Rocky Mountains. Conversely, in the US Pacific Northwest and northern California where ROS historically occurred in the winter at higher elevations, ROS tended to shift towards spring and become less dominant in any given season (Supplementary Fig. 3).

Spatial and ROS event analyses. An analysis of ROS volume changes for the top 10 daily events at the scale of individual river basins was conducted by summing the gridded water available for runoff from each model run to the geographical extent of basins located within the model domain as represented in the North American Atlas – Basin Watersheds data set (http://geogratis.gc.ca/download/frameworkdata/North_America_Atlas10M/watersheds/). For each basin, the total daily ROS volumes for all days were ranked from largest to smallest and the top 10 ROS volumes were summed. The analysis was conducted separately on the historical and warmer scenarios. As such, we did not conduct a comparison of individual storms between the historical and future climates. Rather, we evaluated how the largest events by volume for an individual basin change between the two climate scenarios.

Basins with fewer than 10 events meeting the ROS threshold criteria in either scenario were not evaluated in the top 10 event assessment (see white-coloured basins in Fig. 4). The analysis was conducted for the top-n ROS events, with n ranging from 1 to 9 (not shown); the magnitudes and spatial patterns did not substantially differ from the top 10 events (Fig. 4), but relationships shown in the scatter plots of Fig. 4 became less robust (that is, the data points were more dispersed) with $n < 5$. However, many western Canadian Prairie river basins that did not meet the $n = 10$ threshold did exhibit large ROS event volume increases with $n < 3$ (not shown). The results suggest that future work with simulation periods longer than the 13 years evaluated here is needed and may offer important insight into the changing nature of rare, or extreme, ROS events.

To assess how changes in the spatial extent of ROS events relate to elevation changes, we computed changes in the elevation range of the top 10 ROS events. The basin-wise elevation range was computed as the difference of the maximum and minimum elevation values of pixels satisfying the ROS thresholds within a basin. The metric was computed for each scenario, basin and ROS event, and an average metric was computed for the top 10 events for each basin and scenario. The change in elevation range was computed as the difference in the elevation range between the PGW and historical scenarios. Similarly, we also computed the dates of the top 10 events and the average change in the dates between the PGW and historical scenarios. These change metrics are plotted against changes in total ROS volume (Fig. 4e,f).

Data availability. The data that support the findings of this study are available online (https://rda.ucar.edu/datasets/ds612.0/) and are citable with https://doi.org/10.5065/D6V40SXP. Additional analysis and plotting code is available upon request from the corresponding author.

References

31. Dee, D. et al. The ERA-Interim reanalysis: configuration and performance of the data assimilation system. *Q. J. R. Meteorol. Soc.* **137**, 553–597 (2011).
32. Niu, G.-Y. et al. The community Noah land surface model with multiparameterization options (Noah-MP): 1. Model description and evaluation with local-scale measurements. *J. Geophys. Res.* **116**, D12109 (2011).
33. Jennings, K. S., Winchell, T. S., Livneh, B. & Molotch, N. P. Spatial variation of the rain–snow temperature threshold across the Northern Hemisphere. *Nat. Commun.* **9**, 1148 (2018).
34. Musselman, K. N., Clark, M. P., Liu, C., Ikeda, K. & Rasmussen, R. Slower snowmelt in a warmer world. *Nat. Clim. Change* **7**, 214–219 (2017).
35. Prein, A. F. et al. Increased rainfall volume from future convective storms in the US. *Nat. Clim. Change* **7**, 880–884 (2017).
36. Prein, A. F. et al. The future intensification of hourly precipitation extremes. *Nat. Clim. Change* **7**, 48–52 (2017).
37. Carroll, T. et al. NOHRSC operations and the simulation of snow cover properties for the coterminous U.S. in *Proc. 69th Western Snow Conference* 16–19 (Western Snow Conference, 2001).
38. Musselman, K. N., Pomeroy, J. W., Essery, R. L. & Leroux, N. Impact of windflow calculations on simulations of alpine snow accumulation, redistribution and ablation. *Hydrol. Process.* **29**, 3983–3999 (2015).
39. Wayand, N. E., Marsh, C. B., Shea, J. M. & Pomeroy, J. W. Globally scalable alpine snow metrics. *Remote Sens. Environ.* **213**, 61–72 (2018).
40. Daly, C. et al. Physiographically sensitive mapping of climatological temperature and precipitation across the conterminous United States. *Int. J. Climatol.* **28**, 2031–2064 (2008).
41. Schär, C., Frei, C., Lüthi, D. & Davies, H. C. Surrogate climate-change scenarios for regional climate models. *Geophys. Res. Lett.* **23**, 669–672 (1996).
42. Rasmussen, R. et al. Climate change impacts on the water balance of the Colorado headwaters: high-resolution regional climate model simulations. *J. Hydrometeorol.* **15**, 1091–1116 (2014).
43. Shaw, T. et al. Storm track processes and the opposing influences of climate change. *Nat. Geosci.* **9**, 656–664 (2016).
44. Pendergrass, A. G., Knutti, R., Lehner, F., Deser, C. & Sanderson, B. M. Precipitation variability increases in a warmer climate. *Sci. Rep.* **7**, 17966 (2017).
45. Klein Tank, A. M. G., Zwiers, F. W. & Zhang, X. *Guidelines on Analysis of Extremes in a Changing Climate in Support of Informed Decisions for Adaptation* Report No. 72 (World Climate Data and Monitoring Programme, World Meteorological Organization, 2009).
46. Würzer, S., Jonas, T., Wever, N. & Lehning, M. Influence of initial snowpack properties on runoff formation during rain-on-snow events. *J. Hydrometeorol.* **17**, 1801–1815 (2016).
47. Trubilowicz, J. W. & Moore, R. Quantifying the role of the snowpack in generating water available for runoff during rain-on-snow events from snow pillow records. *Hydrolog. Process.* **31**, 4136–4150 (2017).